Accepted Manuscript

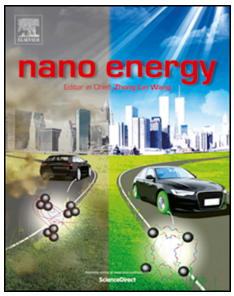

Self-powered on-line ion concentration monitor in water transportation driven by triboelectric nanogenerator

Chen Chen, Zhen Wen, Aimin Wei, Xinkai Xie, Ningning Zhai, Xuelian Wei, Mingfa Peng, Yina Liu, Xuhui Sun, John T.W. Yeow

PII: S2211-2855(19)30435-5

DOI: https://doi.org/10.1016/j.nanoen.2019.05.029

Reference: NANOEN 3743

To appear in: *Nano Energy*

Received Date: 22 March 2019

Revised Date: 24 April 2019

Accepted Date: 10 May 2019

Please cite this article as: C. Chen, Z. Wen, A. Wei, X. Xie, N. Zhai, X. Wei, M. Peng, Y. Liu, X. Sun, J.T.W. Yeow, Self-powered on-line ion concentration monitor in water transportation driven by triboelectric nanogenerator, *Nano Energy* (2019), doi: https://doi.org/10.1016/j.nanoen.2019.05.029.

Graphical Abstract

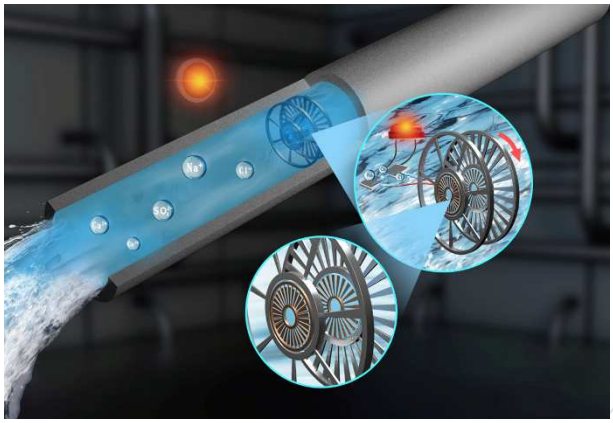

Self-powered on-line ion concentration monitor in water transportation driven by triboelectric nanogenerator

Chen Chen[1,2], Zhen Wen[1,], Aimin Wei[1], Xinkai Xie[1], Ningning Zhai[1], Xuelian Wei[1], Mingfa Peng[1], Yina Liu[3], Xuhui Sun[1,]* and John T. W. Yeow[2,]**

[1] Institute of Functional Nano and Soft Materials (FUNSOM), Jiangsu Key Laboratory for Carbon-Based Functional Materials and Devices, and Joint International Research Laboratory of Carbon-Based Functional Materials and Devices, Soochow University, Suzhou 215123, China.

[2] Advanced Micro-/Nano-Devices Lab, Department of Systems Design Engineering, Waterloo Institute for Nanotechnology, University of Waterloo, 200 University Avenue West, Waterloo, ON, N2L 3G1, Canada.

[3] Department of Mathematical Sciences, Xi'an Jiaotong-Liverpool University, Suzhou 215123 China.

*Corresponding Author E-mail: Z. Wen: wenzhen2011@suda.edu.cn; X. Sun: xhsun@suda.edu.cn; J. T. W. Yeow: jyeow@uwaterloo.ca

ABSTRACT

Ion concentration in water is a key criterion for evaluating water quality. In this work, we developed a self-powered on-line ion concentration monitor in water transportation based on impedance matching effect of triboelectric nanogenerator (TENG). A rotary disc-shaped TENG (RD-TENG) and an ion concentration sensor were fabricated based on the industrial printed circuit board (PCB) technology. Flowing water in the pipeline acts as the energy source to drive the RD-TENG and generate an open-circuit (V_{oc}) of 210 V. The ion concentration sensor exhibits a nearly pure resistance characteristic under the alternating current (AC) signal with the frequency below 500 Hz, corresponding to the rotation speed of 250 rpm for the RD-TENG. The impedance matching relationship between the RD-TENG and ion concentration sensor are experimentally studied and applied to elucidate the sensing mechanism. Finally, a self-powered sensing system integrated with an alarm circuit was assembled which exhibits excellent responsibility and high sensitivity. The change of ion concentration with only 1×10^{-5} mol/L can light up an alarm LED.

KEYWORDS: triboelectric nanogenerator, self-powered, impedance matching effect, ion concentration monitor, on-line

1. Introduction

Water is one of the most indispensable substances not only in daily life but also in industrial production. According to various industrial usage, such as preparation of purified reagent, manufacture of battery related production and cleaning of electronics, different regulations of water quality should be met [1,2]. Excess ions, particles and bacteria may lead to severe problem in industrial production. Although numerous water purification methods have been applied into practice and extremely pure water can be realized [3–6], contamination can still be induced in the transportation of water. It is vitally meaningful to monitor the water quality on-line and in real time during the transportation. In multitudinous factors for evaluating water quality, ion concentration is a symbolic element. Currently, many advanced ion concentration sensors can detect ions in water physically [7–9], chemically [10–12] and biologically [13–15]. Despite high sensitivity, most of existing sensors suffer from complex sensing process and difficulty in real-time monitoring. Another prominent problem in common is power consumption. External energy source is usually required to drive the ionic sensor with an alarm system. When a large number of sensors implanted along the transportation pipeline, it is an enormous engineering effort to provide external electricity.

Among the external electric powers, battery is the most commonly-used way to power the sensors. However, the lifespan of battery limits the long-term usage of the sensing systems [16–18]. If the mechanical energy of water flow can be collected and utilized to drive sensors and alarms, it will be a perfect solution. Nowadays, the emerging triboelectric nanogenerator (TENG) has addressed an approach to actuate multifarious electronic devices by harvesting mechanical energies from ambient [19–21]. Several efforts to achieve TENG-triggered self-powered sensing systems have been made [22–26]. Among them, the most striking strategy is to develop appropriate

TENGs which can drive the existing sensors directly based on the impedance matching effect between the TENGs and sensors [27–31]. In a typical process, the specific output characteristics of the TENG tuned by the load of the sensor is responded to the external stimuli. The output voltage of TENG varies with the different working states of the sensor and can then directly reflect on the on/off status of the alarm unit such as the light of LEDs.

In this work, a TENG driven self-powered on-line monitoring system in the pipeline transportation of water is presented, introducing a new monitoring strategy. A turbo fan driven RD-TENG was proposed to convert the mechanical energy of the flowing water in the pipeline to electrical energy. The RD-TENG was fabricated based on the standard PCB technology. An ion concentration sensor was designed and fabricated also using PCB technology to monitor the ion concentration in water. An alarming electric circuit was designed and built, which consists of a fixed resistor, the sensor and the TENG in series and connected a commercial LED with the fixed resistor in parallel as alarm. The output performance of the TENG was evaluated and the sensing performance of the system was investigated in detail. As a potential application, the reported self-powered sensing system demonstrated the capability of monitoring the ion concentration of pure water under the regulation of semiconductor industry.

2. Results and discussion

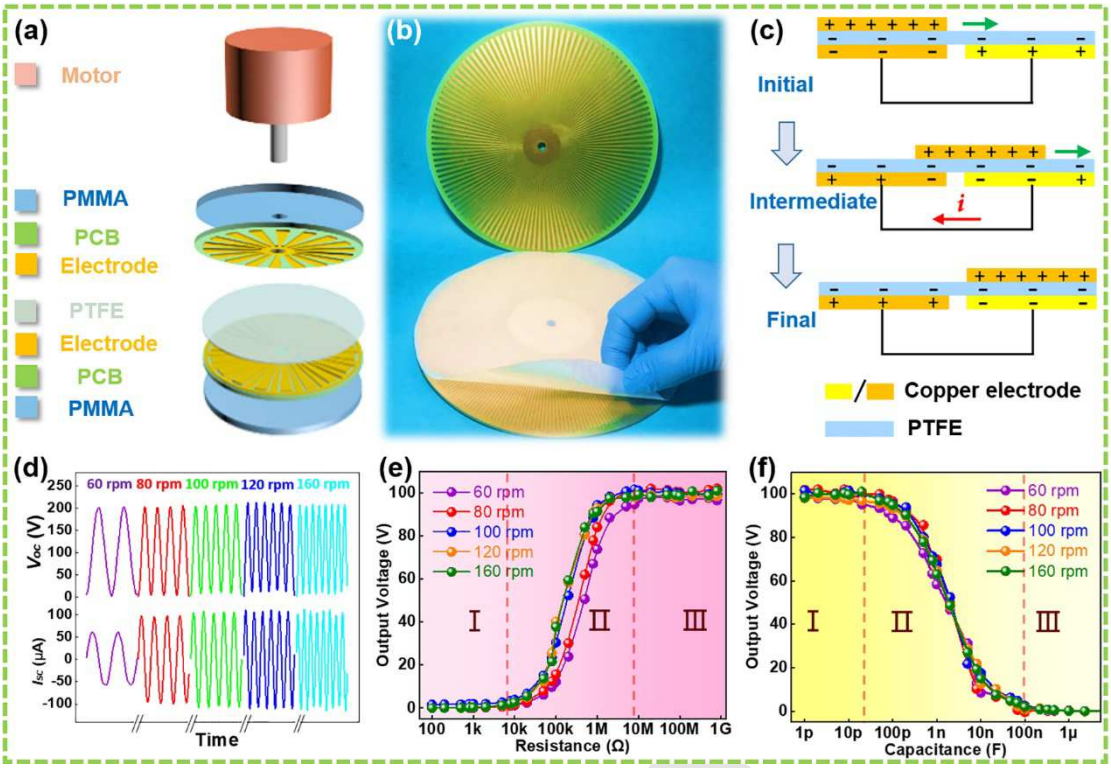

Figure 1. Structure, working mechanism and load output characteristics of a typical rotary disc-shaped triboelectric nanogenerator (RD-TENG). (a) Exploded view and (b) photograph of a typical RD-TENG. (c) Illustration of working mechanism of the RD-TENG. One section of the disc is selected to display the charge distribution during the spinning of the rotator. (d) Open-circuit voltage (V_{oc}) and short-circuit current (I_{sc}) of the RD-TENG at different rotation speeds. Relationship between output voltage and (e) load resistance or (f) load capacitance at different rotation speeds. Three working regions can be defined and marked as Zone I, II and III, respectively.

A typical RD-TENG is usually employed as a high-efficiency energy harvester to collect continuous flow or wind energy, as shown in **Figure 1**a and **1**b. With a multi-layer structure, RD-TENG mainly contains a disk-shaped stator and a countered rotator. For the rotator, the radially copper segments were firstly deposited on a print circuit board (PCB) as one triboelectrification layer. For the stator, arrayed copper segments were properly patterned with two interdigitated structures separated by fine trenches. A PTFE (Polytetrafluoroethylene) thin film was coated atop the copper

electrodes as the other triboelectrification layer. The detailed structure dimensions and fabrication process can be found in the Experimental section.

The operation of the RD-TENG is based on the coupling effects of triboelectrification and electrostatic induction [32–34]. **Figure 1**c demonstrates the charge distribution of the RD-TENG in short-circuit condition for one section in a half cycle. The detailed physical description of the electric generation process can be found in the **Supporting Note 1**. Under the continuous rotation, the current and the inverse current are produced successively and periodically. Consequently, an alternating current (AC) is generated, which has a frequency as

$$f = \frac{3\gamma}{\delta_0} \quad (1)$$

where γ is the rotation speed (rpm) of the disc and δ_0 is the center angle (°) of a single rotator section. Here, δ_0 for the RD-TENG is 1.5°. Figure 1d shows the rotation speed dependence of the electrical output performance. Under the rotation speed of 60, 80, 100, 120 and 160 rpm (controlled by a programmable motor), the open-circuit voltage (V_{oc}) of the RD-TENG almost keeps consistently same and the peak-to-peak value is ~210 V. However, the short-circuit current (I_{sc}) shows a direct proportional dependence on the rotation speed. At the rotation speed of 60 rpm, the I_{sc} is 62 μA. The value approaches the maximum (~112 μA) at the rotation speed of 120 rpm and almost keeps constant even though the rotation speed further increases.

The output voltage of the RD-TENG under different load resistances and capacitances, namely, load output characteristics, has also been thoroughly studied. It is clearly seen that three typical working regions can be divided for both figures, which can be marked as Zone I, II and III, respectively. As shown in Figure 1e, when the load resistance is less than 10 kΩ, the voltage loaded on the external resistor approaches zero and a quasi-short circuit condition is considered (Zone I). When the

load resistance is larger than 10 MΩ, most open-circuit voltage is loaded on the external resistor and a quasi-open circuit condition is considered (Zone III). Within the range of 10 kΩ ~10 MΩ, the output voltage increases from minimum to maximum value rapidly (Zone II). Similarly, the output voltage dependence on external capacitance can also be explained by the limit approximation method, as shown in **Figure 1**f. It drops dramatically when the load capacitance increases from 20 pF to 100 nF. Therefore, the sensing range typically locates in the Zone II for better sensitivity. It can also be observed the output voltage of the RD-TENG with the load resistance is partly dependent on the rotation speed, where the higher rotation speed leads to a faster increase of output voltage. On the contrary, the output voltage of the RD-TENG with the load capacitance is almost independent on the rotation speed. This can be explained by the Ohm's law and the impedance matching effect. In theory, the RD-TENG can be considered as a serial connection of a time-varying capacitance and an ideal voltage source (V_{OC}). There is no resistance term in it. With the maximum output voltage, the instantaneous inherent impedance of the RD-TENG can be expressed as

$$Z_{in} = \frac{1}{2\pi f \cdot C_T} \tag{2}$$

Where f is the frequency of the AC signal (corresponding to rotation speed) and C_T is the instantaneous capacitance of the RD-TENG when the output voltage has the maximum value. When there is only load resistance in the external circuit, the load impedance Z_R is

$$Z_R = R \tag{3}$$

On the contrary, there is no resistance term in the circuit when only load capacitance is connected with the RD-TENG. The load impedance Z_C is defined as

$$Z_C = \frac{1}{2\pi f \cdot C_L} \tag{4}$$

Combining equation 2, 3 and 4, we can obtain the maximum output voltage of the RD-TENG with load resistance and load capacitance:

$$V_R = \frac{Z_R}{Z_{in}+Z_R} \cdot V_{OC} = \frac{R}{\frac{1}{2\pi f \cdot C_T}+R} \cdot V_{OC} \tag{5}$$

$$V_C = \frac{Z_C}{Z_{in}+Z_C} \cdot V_{OC} = \frac{\frac{1}{C_L}}{\frac{1}{C_T}+\frac{1}{C_L}} \cdot V_{OC} \tag{6}$$

According to these two expressions, it is apparent that the output voltage of the RD-TENG with load resistance is dependent on the frequency, or rotation speed. Higher frequency results in a higher output voltage. Meanwhile, the output voltage of the RD-TENG with load capacitance is independent on the frequency.

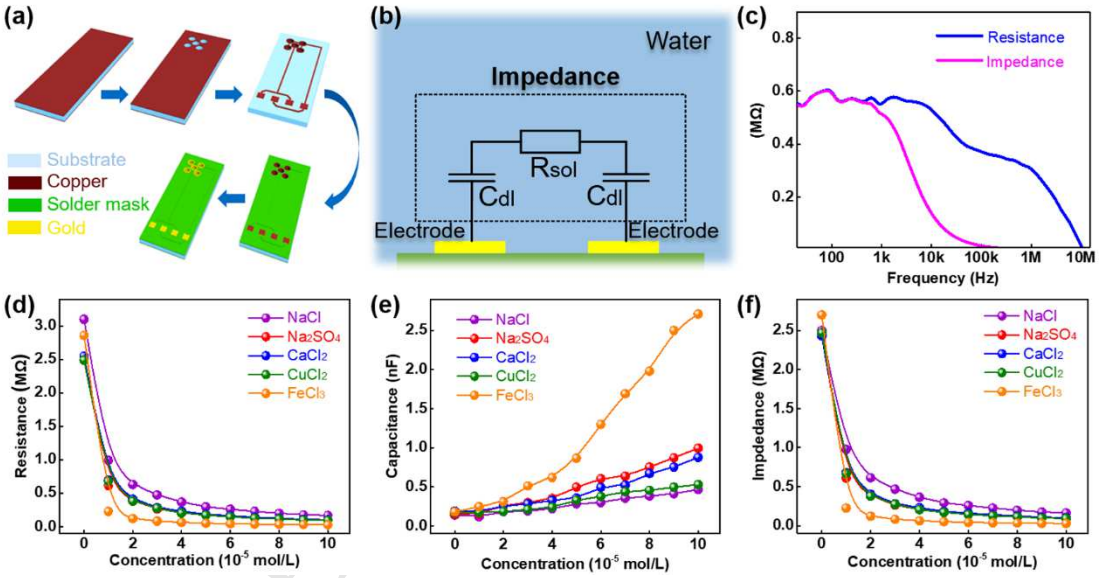

Figure 2. Fabrication, working mechanism and characterizations of an ion concentration sensor. (a) Scheme of the fabrication process of a typical sensor. (b) Working mechanism of the sensor in water. (c) Frequency sweep of resistance and impedance for the sensor in the NaCl solution of 2×10^{-5} mol/L in concentration. Ion concentration dependence of (d) the resistance, (e) the capacitance and (f) the impedance under 200 Hz AC signal drive.

To propose the concept of impedance matching effect of TENG driven self-powered sensing system, a capacitance-type ion concentration sensor was fabricated as an example. **Figure 2**a shows the main steps of the fabrication flow of the ion

concentration sensor that based on the mature industrial PCB fabrication technology. **Figure S1** demonstrates the PCB layout and the photography of the sensor respectively. The sensing mechanism of the ion concentration sensor can be explained by the impedance variation in the water between electrodes under different ion concentrations. **Figure 2**b illustrates the equivalent circuit of the sensor in water. When the sensor is connected with an external source and immersed into the water, an electrical double-layer capacitor forms near the surface of the electrodes. Therefore, the total impedance (Z_{tot}) between electrodes can be approximately defined as:

$$Z_{tot} = R_{sol} + 2X_{Cdl} \quad (7)$$

where R_{sol} is the bulk resistance of the water and X_{Cdl} is capacitive reactance contributed by the electrical double-layer capacitance near the electrode surface. Here, each electrode has two sensing pads connected in parallel for increasing the sensing area (Figure S1b). Both of R_{sol} and X_{Cdl} are dependent on the ion concentration in the water. When the ion concentration changes in the water, the impedance of the sensor will change accordingly. To study the sensing performance, the sensor was immersed into the water with different ion concentrations and the impedance of the sensor was measured. The detailed experimental setup can be found in the Experimental section. After adding two droplets of NaCl solution in the ultra-pure water, correspondingly 2×10^{-5} mol/L, a frequency sweep of resistance and impedance was performed from 20 Hz to 10 MHz, as depicted in **Figure 2**c. The values of impedance and resistance are almost consistent until the frequency reaches 500 Hz, corresponding to the rotation speed of 250 rpm for the RD-TENG. Furthermore, the value of the impedance falls rapidly while the value of the resistance falls much more slowly, because the capacitive reactance contributes very little to the impedance at low frequency (lower than 500 Hz). Numerically, the impedance of the sensor is approximately equal to the

resistance. When the frequency is higher than 500 Hz but lower than 10 MHz, the capacitive reactance cannot be ignored. Therefore, the impedance and the resistance vary. When the frequency is higher than 10 MHz, the impedance nearly approaches zero because the capacitive reactance dominates the impedance. In the case of this RD-TENG, the generated AC power always has a frequency below 500 Hz. In consequence, we can ignore the concept of impedance and use only resistance instead in the following discussion for simplification even though there are reactance components in the circuit. For further verification, the resistance, capacitance and impedance of the sensor immersed in the water, were measured under the frequency of 200 Hz as the ion concentration increases, as depicted in **Figure 2**d, **2**e, and **2**f, respectively. It is obviously shown that, with the increase of the ion concentration, the impedance of the sensor almost follows the trend of the resistance even though the capacitance has the opposite trend. Additionally, the comparisons between the impedance and the resistance under 200 Hz AC signal for NaCl, Na_2SO_4, $CaCl_2$, $CuCl_2$ and $FeCl_3$ are also shown in **Figure S2**. Among these, the curves of the resistance and the impedance are always highly consistent. Moreover, the resistance of the sensor in ultra-pure water is ~3 MΩ, so that the dynamic sensing range of the ion sensor can be roughly considered as ~3 MΩ. Apparently, it can be full overlapped by the Zone II of the RD-TENG (~ 10 MΩ). By properly designing of the structure of TENG, the dynamic sensing range of the sensor can always be located in the Zone II. With tiny change of resistance, the output voltage of the RD-TENG will dramatically change, leading to an extremely high sensitivity.

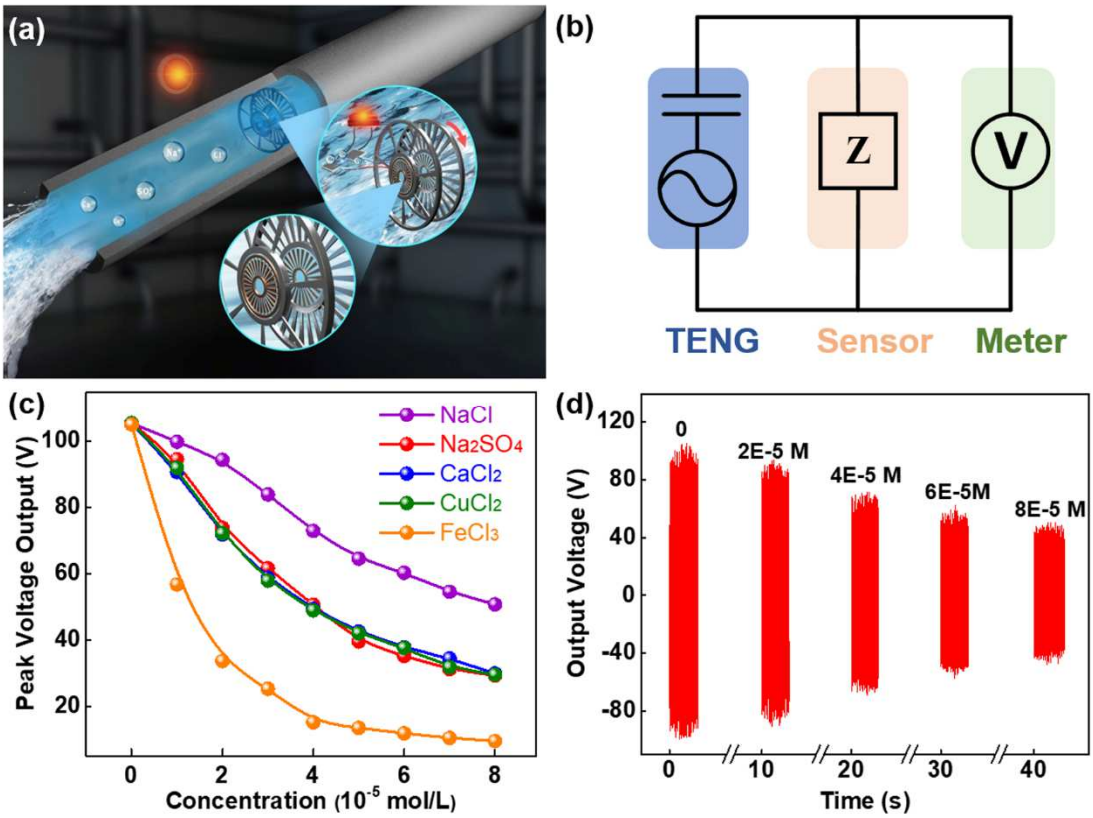

Figure 3. Combination of RD-TENG and ion concentration sensor for self-powered ion concentration monitor system. (a) Schematic illustration of the self-powered sensing system. (b) Equivalent circuit of the experimental setup. (c) Ion concentration dependence of the peak output voltage for different aqueous solutions. (d) Real-time output voltage of the RD-TENG when the sensor immersed in the NaCl aqueous solutions with different concentrations.

Based on the above results, we further proposed a TENG driven self-powered on-line monitoring system in the pipeline transportation of water, as illustrated in **Figure 3**a. In this system, a packaged RD-TENG is attached to a turbo fan, driven by flowing water in the pipeline. And then the ion concentration sensor, immersed in the water, and an alarm component are connected in series with the RD-TENG to form a self-powered sensing system, which enables to convert mechanical energy of the flowing water into electricity to power the ion concentration sensor and alarm. When the ion concentration in the water pipeline has a tiny increase, the alarm will respond immediately. **Figure 3**b illustrates the equivalent circuit for the electrical

measurements of the self-powered sensing system. A source meter was connected in parallel with the sensor to measure the output voltage of the RD-TENG under the rotation speed of 100 rpm. **Figure 3**c illustrates the change of the peak output voltage on the ion concentration sensor as the ion concentration increases. Five different prepared solutions (NaCl, Na_2SO_4, $CaCl_2$, $CuCl_2$ and $FeCl_3$, 0.1 mol/L) were added into ultra-pure water drop by drop (15 μL per drop), respectively, to obtain different ion concentrations. The peak output voltage suggests an inversely proportional relation with the ion concentration. Among all of these five curves, the output voltage starts from 105 V, which corresponds to the V_{oc} of the RD-TENG. The NaCl curve is most linear and falls most slowly while the $FeCl_3$ curve is most nonlinear and falls fastest. Na_2SO_4, $CaCl_2$ and $CuCl_2$ curves are between NaCl curve and $FeCl_3$ curve. In addition, these three curves are highly overlapped. It can be explained by the total charge concentration (positive charges plus negative charges) of different substances. For example, the solutions with 1 μmol/L of NaCl, Na_2SO_4, $CaCl_2$, $CuCl_2$ and $FeCl_3$, the total charge concentration of the free charges is 2, 4, 4, 4 and 6 μmol/L, respectively. With same concentration, NaCl causes the worst conductivity (the highest resistance) while $FeCl_3$ causes the best conductivity (the lowest resistance). Correspondingly, the NaCl curve has the mildest slope while the $FeCl_3$ curve has the wildest slope. According to this ion concentration dependence of the output voltage of the RD-TENG, a self-powered ion concentration sensor can be realized. **Figure 3**d shows the real-time output voltage on the ion concentration sensor when the sensor immersed in the water with different NaCl concentrations. It should be noted that the impedance of the ion concentration sensor in aqueous solution is almost independent on the frequency under 500 Hz. On the contrary, the inherent impedance of the RD-TENG is theoretically is related to the rotation speed [35]. **Figure S**3 shows the ion

concentration dependence of the peak output voltage for NaCl aqueous solution with different rotation speed. It is observed that the peak output voltage drops faster with lower rotation speed, which can be explained by equation 5. Although the rotation speed, corresponding to flowing speed of the water in pipeline, has a significant effect of the output voltage on the ion concentration, the system can still achieve the sensing function.

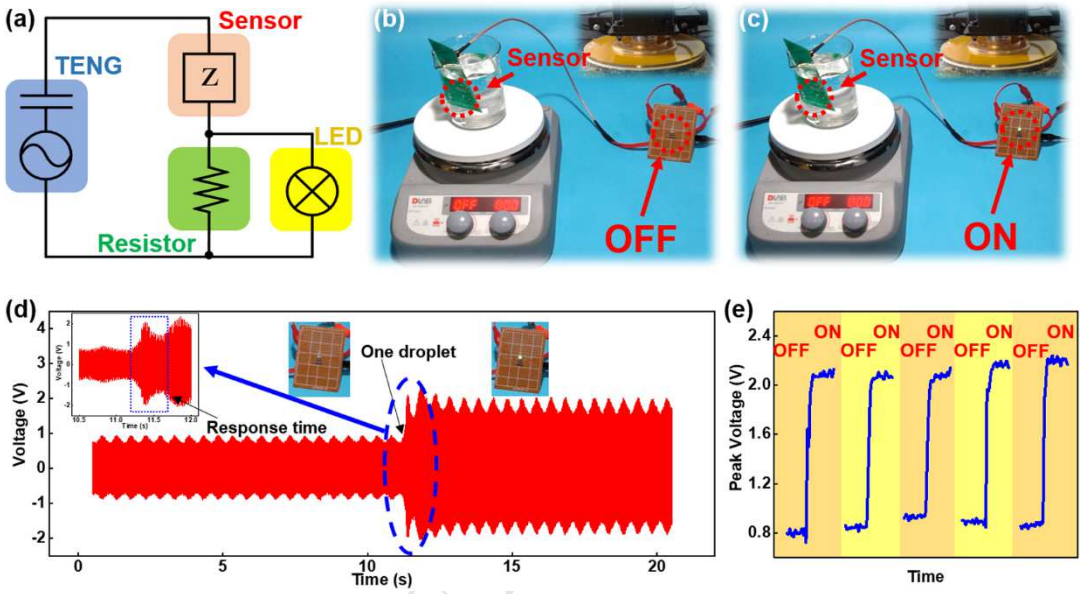

Figure 4. Demonstration of the self-powered ion concentration monitor system. (a) Equivalent circuit for demonstrating the application of monitoring the water quality. Alarm LED is (b) OFF for the ultra-pure water, and (c) lighted/ON with one droplet of 0.1 mol/L NaCl solution. (d) Real-time voltage response between the alarm LED during the experiment. Inset: response time of the sensing alarm system. (e) Reliability test of the sensing alarm system for 5 cycles.

To bring the sensing system into practical application, a proper circuit was designed and a real self-powered sensing alarming system was built for demonstration, as demonstrated in **Figure 4**a. Herein, a beaker filled with 150 mL ultra-pure water is positioned on a magnetic stirrer. The stirrer is to accelerate the mixing of the ion solution. The sensing areas of the sensor is immersed into the water. The NaCl solution of 0.1 mol/L had been prepared in advance. A fixed resistor (150

kΩ) was connected in series with the sensor to control the output voltage of the RD-TENG. A commercial LED (threshold voltage: 1.4 V), in parallel connection with the fixed resistor, was used to realize the alarm function. To simulate the scenario that the turbo fans drive the RD-TENG, a motor was utilized to actuate the rotator of the RD-TENG and the control the rotation speed. The rotation speed was set to 100 rpm, corresponding to an AC power with frequency of 200 Hz. Initially, the LED is in the state of OFF, as shown in Figure 4b. Then, one droplet of NaCl solution (15 μL) is added into the ultra-pure water and the LED turns on instantly (shown in **Figure 4**c). Supporting Movie S1 shows the process of monitoring the water quality. **Figure 4**d shows the real-time voltage response of the LED during the experiment. We can clearly see that the peak voltage output on the LED increases from 0.9 V to 2 V rapidly after adding one droplet of NaCl solution. The inserted figure is the enlarged view of the circled region. It is illustrated that the response time of the sensing system is in the scale of millisecond. As abovementioned, the capacitive reactance contributes very little to the variation of the impedance of the sensor at this low working frequency. Hence, the change of the capacitive reactance with the ion concentration is not considered and all of the electrical components in the circuit are considered as pure resistors for this alarm system. When the ion concentration increases in the water, the conductivity of the water increases, leading to the decrease of resistance between electrodes of sensor. The output voltage (V_{LED}) on the LED is defined:

$$V_{LED} = \frac{R_{fix}}{R_{fix}+R_{sensor}} V_0 \quad (8)$$

where R_{fix} is the resistance of the fixed resistor, R_{sensor} is the resistance of the sensor, and V_0 is the output voltage of the RD-TENG with the load resistance of (R_{fix}+R_{sensor}). Although the output voltage of the RD-TENG decreases as the increase of the ion

concentration in the water, the value is still much higher than the threshold of a commercial LED. Therefore, the voltage on the LED still increased as the ion concentration increases in the water. To study the reliability of the self-powered sensing alarm system, we performed the alarming experiments for several times. After each cycle of experiment, we rinsed the ion concentration sensor and replaced the water in the beaker with fresh ultra-pure water. Then, we repeated the experiment again. Every time, we measured the peak output voltage on the LED. The peak voltage vs. time was plotted, as depicted in Figure 4e. It shows that the peak voltage on the LED is consistently lower than the threshold voltage (1.4 V) of the LED before the addition of NaCl solution, while the peak voltage on LED is always higher than the threshold after the addition of NaCl solution. Hence, the self-powered sensing alarm system exhibits excellent reliability. Currently, most foundries follow the standard guides given by American Society for Testing Materials (ASTM) for pure water in electronics and semiconductor industries. Various and detailed limits are defined for pure water with respect to the line width of the devices. **Table S1** shows some requirements of the pure water with different levels in the electronics and semiconductor industries. A typical criterion of the pure water in electronic-grade industry is the concentration of certain ions. For example, the concentration of sodium and chloride should be both lower than 1000 μg/L, corresponding to 2.86×10^{-5} mol/L and 4.35×10^{-5} mol/L, respectively. Therefore, the reported self-powered ion concentration sensing system based on RD-TENG demonstrates the capability of on-line monitoring the water quality with a high sensitivity (1×10^{-5} mol/L), which fully satisfies the requirements in industry.

3. Conclusion

In summary, the RD-TENG driven self-powered sensing system for on-line monitoring of ion concentration in water was proposed. This new sensing strategy can convert the mechanical energy from flowing water in pipeline to electrical energy to power a sensing alarm system, realizing high sensitivity, low cost and low external consumption. Both RD-TENG and ion concentration sensor are designed and manufactured based on the industrial PCB technology, which gives the possibility to integrate them together for further simplification. The output voltage of the RD-TENG shows an independence on rotation speed, where the open-circuit is 210 V. At the working rotation speed (around 100 rpm), the impedance of the sensor in the water can be simply considered as a pure resistance. The relationship between the peak output voltage of the RD-TENG and the ion concentration was studied and the sensor showed excellent responsibility. A demonstration of self-powered sensing alarm system is successfully presented. The change of ion concentration with only 1×10^{-5} mol/L can light up an alarm LED and excellent reliability of the measurement was verified. Furthermore, improvements can still be taken to enhance the performance of the self-powered system, such as the interdigitated-electrode structure for higher sensitivity and proper coating of the electrodes for better selectivity.

4. Experimental

4.1 Structure Dimensions and Fabrication of RD-TENG. The fabrication of the RD-TENG is based on the mature industrial PCB manufacturing technology. For the stator, two copper segments with interdigitated structure were patterned on the PCB. The radially interdigitated copper segments have diameters of 176 mm and 184 mm, respectively. A PTFE thin film, treated by plasma reaction ion etching (RIE) process for enhancing the surface charge density, was coated on the copper electrodes. For the rotator, radial copper segments with a central angle of 1.5° and a thickness of ~70 μm

was patterned on the PCB. For both stator and rotator, PCB was adhered to a stack of acrylic (Polymeric Methyl Methacrylate) sheets to strengthen the structure. A motor was utilized to drive the rotator and the rotator and stator are aligned coaxially in operation.

4.2 Fabrication of Ion Concentration Sensor. The fabrication started from a circuit board substrate cladded by copper. The next step is the drilling of holes in the substrate for Sub-Miniature-A (SMA) connector. Then, the entire surface, including the inside of the holes, of the circuit board was metalized. Proper photolithography process was carried out to pattern the circuit board. The conducting lines and sensing pads were formed. Afterwards, the surface of the circuit board was covered by solder mask lacquer for insulation. Only holes and sensing areas were exposed. The last step was gold immersion to deposit a gold thin film on the surface of sensing pads.

4.3 Impedance Measurements. The impedance of the sensor with different ion concentration was measured under the impedance analyzer (WK, 6500B). 0.1 mol/L NaCl, Na_2SO_4, $CaCl_2$, $CuCl_2$ and $FeCl_3$ solution were prepared and five measurements under different frequencies (10 Hz, 100 Hz, 200 Hz, 1 kHz and 10 kHz) were conducted. Initially, the sensor was connected with the impedance analyzer with a coaxial cable. A beaker filled with ultra-pure water (150 mL) was positioned on a magnetic stirrer, for accelerating the mixing, and the sensing area of the sensor was immersed in the ultra-pure water. The prepared ion solution was added into the ultra-pure water drop by drop (15 μL). A low-level AC driving signal was applied to the sensor, resistance, capacitance and impedance were directly read from the impedance analyzer in real time.

4.4 Electrical Measurements. The electrical measurements of the sensing system were carried out to study the output voltage of the RD-TENG when the sensor

immersed into water with different ion concentration. A source meter (Keithley 6514) was utilized to measure the output voltage. The source meter was connected to a laptop through a data acquisition card (National Instruments, BNC-2110) and a customized data acquisition system based on Labview platform was used to collect the voltage and current signals.

Acknowledgement

This work is supported by the National Science and Engineering Research Council (NEERC) and Canada Research Chairs program (CRC). The work is also supported by National Natural Science Foundation of China (NSFC) (No. 61804103), National Key R&D Program of China (No. 2017YFA0205002), Natural Science Foundation of the Jiangsu Higher Education Institutions of China (No. 18KJA535001, No. 14KJB150020), Natural Science Foundation of Jiangsu Province of China (No. BK20170343, BK20180242), China Postdoctoral Science Foundation (No. 2017M610346), Collaborative Innovation Center of Suzhou Nano Science & Technology, the Priority Academic Program Development of Jiangsu Higher Education Institutions (PAPD) and the 111 Project.

Notes

The authors declare no competing financial interest.

Appendix A. Supporting information

Supplementary data associated with this article can be found in the online version at doi:10.1016/j.nanoen.2019.

Reference

[1]T. Ehmann, C. Mantler, D. Jensen, R. Neufang, Monitoring the quality of ultra-pure water in the semiconductor industry by online ion chromatography, Microchim. Acta. 154 (2006) 15–20.

[2]W.H. Organization, Guidelines for drinking-water quality, World Health Organization, 2004.

[3]N. Savage, M.S. Diallo, Nanomaterials and water purification: opportunities and challenges, J. Nanoparticle Res. 7 (2005) 331–342.

[4]R.A. Khaydarov, R.R. Khaydarov, O. Gapurova, Water purification from metal ions using carbon nanoparticle-conjugated polymer nanocomposites, Water Res. 44 (2010) 1927–1933.

[5]T.S. Sreeprasad, S.M. Maliyekkal, K.P. Lisha, T. Pradeep, Reduced graphene oxide–metal/metal oxide composites: facile synthesis and application in water purification, J. Hazard. Mater. 186 (2011) 921–931.

[6]S. Bolisetty, R. Mezzenga, Amyloid–carbon hybrid membranes for universal water purification, Nat. Nanotechnol. 11 (2016) 365.

[7]M.A. Shenashen, S.A. El-Safty, E.A. Elshehy, Architecture of optical sensor for recognition of multiple toxic metal ions from water, J. Hazard. Mater. 260 (2013) 833–843.

[8]A.I. Zia, A.R.M. Syaifudin, S.C. Mukhopadhyay, P.L. Yu, I.H. Al-Bahadly, C.P. Gooneratne, J. Kosel, T.-S. Liao, Electrochemical impedance spectroscopy based MEMS sensors for phthalates detection in water and juices, in: J. Phys. Conf. Ser., IOP Publishing, 2013: p. 12026.

[9]G. Sener, L. Uzun, A. Denizli, Colorimetric sensor array based on gold nanoparticles and amino acids for identification of toxic metal ions in water, ACS Appl. Mater. Interfaces. 6 (2014) 18395–18400.

[10]I.-B. Kim, U.H.F. Bunz, Modulating the sensory response of a conjugated polymer by proteins: an agglutination assay for mercury ions in water, J. Am. Chem. Soc. 128 (2006) 2818–2819.

[11]L. Sartore, M. Barbaglio, L. Borgese, E. Bontempi, Polymer-grafted QCM chemical sensor and application to heavy metal ions real time detection, Sensors Actuators B Chem. 155 (2011) 538–544.

[12]F. Tan, L. Cong, N.M. Saucedo, J. Gao, X. Li, A. Mulchandani, An electrochemically reduced graphene oxide chemiresistive sensor for sensitive detection of Hg2+ ion in water samples, J. Hazard. Mater. 320 (2016) 226–233.

[13]C. Chouteau, S. Dzyadevych, C. Durrieu, J.-M. Chovelon, A bi-enzymatic whole cell conductometric biosensor for heavy metal ions and pesticides detection in water samples, Biosens. Bioelectron. 21 (2005) 273–281.

[14]H. Guedri, C. Durrieu, A self-assembled monolayers based conductometric algal whole cell biosensor for water monitoring, Microchim. Acta. 163 (2008) 179–184.

[15]F. Long, A. Zhu, H. Shi, H. Wang, J. Liu, Rapid on-site/in-situ detection of heavy metal ions in environmental water using a structure-switching DNA optical biosensor, Sci. Rep. 3 (2013) 2308.

[16]Z.L. Wang, J. Chen, L. Lin, Progress in triboelectric nanogenerators as a new energy technology and self-powered sensors, Energy Environ. Sci. 8 (2015) 2250–2282.

[17]Z. Wen, M.-H. Yeh, H. Guo, J. Wang, Y. Zi, W. Xu, J. Deng, L. Zhu, X. Wang, C. Hu, Self-powered textile for wearable electronics by hybridizing fiber-shaped nanogenerators, solar cells, and supercapacitors, Sci. Adv. 2 (2016) e1600097.

[18]Y. Liu, N. Sun, J. Liu, Z. Wen, X. Sun, S.-T. Lee, B. Sun, Integrating a silicon solar cell with a triboelectric nanogenerator via a mutual electrode for harvesting energy from sunlight and raindrops, ACS Nano. 12 (2018) 2893–2899.

[19]F.-R. Fan, Z.-Q. Tian, Z. Lin Wang, Flexible triboelectric generator, Nano Energy. 1 (2012) 328–334.

[20]Z.L. Wang, On Maxwell's displacement current for energy and sensors: the origin of nanogenerators, Mater. Today. 20 (2017) 74–82.

[21]Z.L. Wang, Nanogenerators, self-powered systems, blue energy, piezotronics and piezo-phototronics–A recall on the original thoughts for coining these fields, Nano Energy. 54 (2018) 477–483.

[22]A. Wei, X. Xie, Z. Wen, H. Zheng, H. Lan, H. Shao, X. Sun, J. Zhong, S.T. Lee, Triboelectric Nanogenerator Driven Self-Powered Photoelectrochemical Water Splitting Based on Hematite Photoanodes, ACS Nano. 12 (2018) 8625–8632.

[23]X. Cao, Y. Jie, N. Wang, Z.L. Wang, Triboelectric nanogenerators driven self□powered electrochemical processes for energy and environmental science, Adv. Energy Mater. 6 (2016) 1600665.

[24]C. Wu, A.C. Wang, W. Ding, H. Guo, Z.L. Wang, Triboelectric Nanogenerator: A Foundation of the Energy for the New Era, Adv. Energy Mater. 9 (2019) 1802906.

[25]X. Pu, H. Guo, J. Chen, X. Wang, Y. Xi, C. Hu, Z.L. Wang, Eye motion triggered self-powered mechnosensational communication system using triboelectric nanogenerator, Sci. Adv. 3 (2017) e1700694.

[26]H. Guo, X. Pu, J. Chen, Y. Meng, M.-H. Yeh, G. Liu, Q. Tang, B. Chen, D. Liu, S. Qi, A highly sensitive, self-powered triboelectric auditory sensor for social robotics

and hearing aids, Sci. Robot. 3 (2018) 2516.

[27]Z. Wen, Q. Shen, X. Sun, Nanogenerators for self-powered gas sensing, Nano-Micro Lett. 9 (2017) 45.

[28]Z. Wen, J. Fu, L. Han, Y. Liu, M. Peng, L. Zheng, Y. Zhu, X. Sun, Y. Zi, Toward self-powered photodetection enabled by triboelectric nanogenerators, J. Mater. Chem. C. 6 (2018) 11893–11902.

[29]Z. Wen, J. Chen, M.-H. Yeh, H. Guo, Z. Li, X. Fan, T. Zhang, L. Zhu, Z.L. Wang, Blow-driven triboelectric nanogenerator as an active alcohol breath analyzer, Nano Energy. 16 (2015) 38–46.

[30]Q. Shen, X. Xie, M. Peng, N. Sun, H. Shao, H. Zheng, Z. Wen, X. Sun, Self-Powered Vehicle Emission Testing System Based on Coupling of Triboelectric and Chemoresistive Effects, Adv. Funct. Mater. 28 (2018) 1703420.

[31]X. Xie, Z. Wen, Q. Shen, C. Chen, M. Peng, Y. Yang, N. Sun, P. Cheng, H. Shao, Y. Zhang, Q. Zhu, X. Chen, X. Sun, Impedance Matching Effect between a Triboelectric Nanogenerator and a Piezoresistive Pressure Sensor Induced Self-Powered Weighing, Adv. Mater. Technol. 3 (2018) 1800054.

[32]G. Zhu, J. Chen, T. Zhang, Q. Jing, Z.L. Wang, Radial-arrayed rotary electrification for high performance triboelectric generator, Nat Commun. 5 (2014) 3426. doi:10.1038/ncomms4426.

[33]S. Niu, S. Wang, Y. Liu, Y.S. Zhou, L. Lin, Y. Hu, K.C. Pradel, Z.L. Wang, A theoretical study of grating structured triboelectric nanogenerators, Energy Environ. Sci. 7 (2014) 2339–2349.

[34]W. Hu, X. Wei, L. Zhu, D. Yin, A. Wei, X. Bi, T. Liu, G. Zhou, Y. Qiang, X. Sun, Enhancing proliferation and migration of fibroblast cells by electric stimulation based on triboelectric nanogenerator, Nano Energy. 57 (2019) 600–607.

[35]S. Niu, Z.L. Wang, Theoretical systems of triboelectric nanogenerators, Nano Energy. 14 (2015) 161–192.

Research Highlights

- Both the ion concentration sensor and the RD-TENG are designed and fabricated based on PCB techniques.
- The open-circuit voltage and the short-circuit current of the RD-TENG can reach up to 210 V and 112 μA, respectively.
- The frequency dependence of the impedance matching effect was studied experimentally.
- Change of 1×10^{-5} mol/L ion concentration can be monitored by the proposed sensing system.